HHS Public Access

Author manuscript

Wiley Interdiscip Rev Nanomed Nanobiotechnol. Author manuscript; available in PMC 2017 November 01.

Published in final edited form as:

Wiley Interdiscip Rev Nanomed Nanobiotechnol. 2016 November ; 8(6): 872–890. doi:10.1002/wnan.1402.

Nanoparticles and Radiotracers: Advances toward Radio-Nanomedicine

Edwin C. Pratt[1], **Travis M. Shaffer**[2,3,4], and **Jan Grimm**[1,2,3,5]

[1]Department of Pharmacology, Weill Cornell Medical College, New York, NY 10021, USA

[2]Department of Radiology, Memorial Sloan Kettering Cancer Center, New York, NY 10065, USA

[3]Molecular Pharmacology Program, Memorial Sloan Kettering Cancer Center, New York, NY 10065, USA

[4]Department of Chemistry, Hunter College and Graduate Center of the City University of New York, New York, NY 10065, USA

[5]Department of Radiology, Weill Cornell Medical College, New York, NY 10021, USA

Abstract

Here, we cover the convergence of radiochemistry for imaging and therapy with advances in nanoparticle (NP) design for biomedical applications. We first explore NP properties relevant for therapy and theranostics and emphasize the need for biocompatibility. We then explore radionuclide-imaging modalities such as Positron Emission Tomography (PET), Single Photon Emission Computed Tomography (SPECT), and Cerenkov Luminescence (CL) with examples utilizing radiolabeled NP for imaging. PET and SPECT have served as diagnostic workhorses in the clinic, while preclinical NP design examples of multimodal imaging with radiotracers show promise in imaging and therapy. CL expands the types of radionuclides beyond PET and SPECT tracers to include high-energy electrons (β^-) for imaging purposes. These advances in radionanomedicine will be discussed, showing the potential for radiolabeled NPs as theranostic agents.

Introduction to Nanomaterials

In biomedical imaging, nanoparticles (NPs) can provide or enhance the distinction of normal from diseased tissue, whether that be tumor margins for image guided surgery, sentinel lymph node drainage in metastatic cancer, or even identifying sites of inflammation. Traditionally, radiotracers have been attached to small molecules or antibodies with the aim of identifying sites of disease as well as diagnostic markers to show efficacy of a particular therapy. In cancer therapy, ideally these radiolabeled agents exhibit additional therapeutic properties, which can be either drugs or radionuclides (e.g. ^{90}Y or ^{177}Lu). NPs have also

Author Contributions

E.C.P., T.M.S. and J.G. wrote and edited the manuscript.

Competing Financial Interests statement

The authors declare no competing financial interests.

emerged as clinically relevant platforms not only for radiotracers, but also as therapeutic agents. While much remains to be discovered about the toxicology of NPs compared to the larger bulk state for a given material, it is known through preclinical studies that some NPs can be taken up in tumors via an upregulated micropinocytosis mechanism, providing a window for imaging and therapy optimization in tumors.[1] Functionalizing unlabeled NPs with affinity tags for specific receptor handshakes can enrich NPs at the desired target. Tethering of imaging agents to NPs such as radioisotopes enables tracking the distribution in vivo through methods such as PET, SPECT, or CL. While many NPs for imaging exist in the preclinical space, few have advanced into the clinic. Designing NPs with mechanisms for endocytosis and endosomal escape to intracellular targets are hallmark challenges in NP delivery systems. Radiolabeled NPs, with high specific activity, advantageously can be used for imaging, minimizing particles necessary for imaging a particular tissue feature. Furthermore, NPs have the potential to carry high levels of radioactivity per particle providing directed internal radiotherapy when targeted. Imaging agents that are simultaneously therapeutic are known as theranostics. In the case of the β^- radionuclides used for CL imaging such as ^{177}Lu and ^{90}Y, the radionuclide is both the imaging agent as well as the therapeutic, though other radionuclides could be used in combination with therapeutic NPs to achieve a theranostic agent.

NP properties are critical to the successful biodistribution of an imaging agent, and if chosen improperly, can lead to off target delivery and toxicity. Classically for small molecules, understanding the uptake and biodistribution is dependent on physiochemical parameters often described as “Lipinski’s rule of Five”[2], covering guidelines such as fewer than 5 hydrogen bond donors, fewer than 10 hydrogen bond acceptors, a molecular mass less than 500 daltons, and partition coefficient greater than 5. Lipinski’s rules were established to achieve drugs with Absorption, Distribution, Metabolism, and Excretion (ADME) sufficient to reach the target while limiting off target effects and extreme delivery methods. In stark contrast, NPs are entities of a much larger order of magnitude and their biodistribution is dependent on entirely different properties such as size, aspect ratio, charge, stiffness, and surface chemistry (determining the properties of the NP’s coating).[3] Furthermore, particle opsonization serves as an elimination mechanism for NPs rather than a depot as seen in plasma bound small molecules which protect the small molecule from direct renal elimination or metabolism. Through the advances in material science and bioengineering, NPs with bio-relevant properties have emerged to better direct the biodistribution of NPs for selective radioimaging and therapy.

A material is considered a NP when at least one dimension is on the order of 10 to 100 nm. NP are synthesized through various methods, which predominantly include bottom up synthesis of liposomes,[4] micelles,[5] polymersomes,[6] dendrimers,[7] carbon nanotubes,[8] and inorganic NPs[9] for example. Many NPs in use today are spherical, though rods, tubes, disks, and worms also are also used in vivo. The variation in morphology is driven by several parameters, mainly by concentrations of lipid or polymer energetics for assembly, the packing parameter of the coating monomer used, and the size of the NP core in the case of a stiff core like metallic NPs (e.g. iron oxide NPs or IONPs, gold NPs or quantum dots). By altering the chemical composition of the lipid or polymer used a wide variety of particles can be achieved, from micelles to worms to multi-lamellar vesicles of varying sizes.[10]

Different size ranges have vastly different biodistributions based on mammalian physiology and serve as the first important parameter in NP design.[3] Particles less than 5nm are rapidly cleared via renal excretion, while particles under 100 nm have shown widespread biodistribution across various organs.[11] Larger particles of several hundred nm begin to restrict NP distribution to the RES (mainly liver and spleen), with micron size particles resulting in undesired residence in capillary beds.

Beyond size, NP shape and charge are key parameters affecting internalization rates of NPs where rod shaped, and positively charged particles were found to result in the greatest uptake in-vitro.[12] NPs with rod-like morphology have been shown to have higher specific and lower nonspecific targeting in vivo compared to identical spherical particles.[13] Furthermore, carbon nanotubes with extremely high aspect ratios and lengths of 200–300 nm have been shown to clear through the kidneys despite having a dimension much greater than the glomerular filtration cutoff. This paradoxical phenomenon is thought to occur by flow orientation of the carbon nanotube tip first through the glomerulus despite the carbon nanotube having a molecular weight 10–20 times the traditional limit for glomerular filtration.[14] Through tuning the size, shape and charge of the NP, tumor uptake can be favored. Furthermore tumors that show uptake of NPs do not necessarily show cellular uptake distribution within the tumor. Ex-vivo analysis by flow of PRINT particles revealed variation in tumor population uptake based upon particle size with macrophages and other leukocytes representing the largest populations taking up NPs aside from cancer cells.[15] Identifying the right subtumoral cell population to target can mean the difference between tracking macrophages to cancer cell labeling and therapy.

Delivery of NPs has often relied on Enhanced Permeability and Retention (EPR) to describe passive but selective delivery to tumors with leaky vasculature.[16] More recently, EPR effects on spontaneous solid canine tumors were imaged using liposomes radiolabeled with $[^{64}Cu]^{2+}$, which exhibited rapid uptake into liposomes. Of the canine tumors tested, an EPR effect was seen in carcinomas but not in sarcomas. This tumor type dependent uptake without a targeting strategy shows not all tumors are amendable to EPR-dependent deliveries nor respond favorably to untargeted NP administration.[17] Where EPR is weak, NPs should be amenable to active targeting and uptake strategies such as sonoporation[18] to enable permeation beyond the vasculature and into the tumor environment. For strictly imaging NPs, cellular uptake is not essential to register location but should have a high enough diffusion to identify tumor margins before the desired imaging time.

As NPs have high surface area to volume ratios, NPs have become ideal platforms upon which surface charge, polymeric coating, and specific targeting ligands can be added to shape the NP biodistribution, reduce nonspecific uptake, and mimic a biological handshake. Targeting ligands for surface conjugation and adsorption can include small molecules,[19] peptides,[20] aptamers,[21,22] and antibodies,[23] Furthermore, attachment of radiotracers via chelators (for radiometal incorporation), prosthetic groups (e.g., for radiohalogen functionalization) may alter NP properties compared to unlabeled NPs. To address this NP alteration, various methods of radiolabeling with NP surface modification have been devised, and are typically referred to as “chelator-free” radiolabeling.[24]

Newer NPs with targeting ligands on the surface have improved delivery to the site of interest. Use of stealth-like coatings such as Polyethylene Glycol (PEG) have been widely used as a passive stealth mechanism,[25] but is not impervious to opsonization in vivo and therefore phagocytosis by the Reticuloendothelial System (RES). Biological coatings that elicit a more active recognition have been utilized, such as CD47 coated NPs which show longer persistence ratios in vivo compared to PEG and similarly opsonized NPs.[26] NP design is moving to include more active targeting of a diseased system while avoiding unwanted phagocytosis by the Mononuclear Phagocytic System (MPS).

Another area not often considered in NP design is the effect of particle stiffness on biodistribution. Comparing equally opsonized soft and stiff NPs showed a greater phagocytic index for stiff particles. The stiffness of the particles could override a “don’t eat me” signal provided by surface bound CD47.[27,28] Therefore, softer NPs and coatings could have an advantage in avoiding off-target uptake. Polymeric coatings in this instance can alter the stiffness of the particle while at the same time serving as a small molecule drug depot and radionuclide anchor. Through deliberate NP design, NPs can be ideal platforms for a variety of radiotracers. With the combination of other imaging agents and targeting moieties, imaging agents and theranostics can be produced with high selectivity from simple NP scaffolds while more complicated structures can enable multimodal imaging and therapy.

Nanoparticles used in nuclear imaging

Many of the lipidic, polymeric, carbonaceous and inorganic NP platforms available are amenable to chemical conjugation for radiolabeling through either direct methods or chelation. Choice of radionuclide depends on the desired duration of the imaging agent, as well as the desired type of imaging intrinsic to the radionuclide decay. Radionuclides that are facile for synthetic routes include ^{11}C, ^{18}F, ^{76}Br and ^{124}I while other radionuclides such as ^{64}Cu, ^{68}Ga, ^{89}Zr, ^{90}Y, ^{99m}Tc, and ^{177}Lu are best attached via chelation or chelator-free surface adsorption.

Liposomes have been widely used with radiotracers and are one of the oldest NP platforms. Morgan and co-workers pioneered multilamellar vesicles with ^{99m}Tc via reduction of pertechnetate in the presence of liposomes in 1981.[29] Liposomes are traditionally made through hydration of lipid films and extrusion through successively smaller membranes to yield sub 200nm NPs with a low polydispersity index. Liposomes have been functionalized with various radiotracers resulting in free activity sequestered to the liposome bilayer or contained in a functionalized chelator. Polymeric NPs can also be radiolabeled using similar methods.

Compared to liposomes and polymersomes, inorganic NPs are stiff core particles that are often made of silica via the Stöber method, but also include a wide variety of semiconducting quantum dots that can be used for multimodal imaging. Furthermore “Cornell Dots” (C dots) have also been synthesized which are either fluorescent[30] or radiolabeled.[31] Other inorganic NPs such as gold and iron oxide have been extensively used for Surface Enhanced Raman Scattering (SERS)[32] as well as MR-weighted contrast

agents.[33] Carbon nanotubes (CNT) have also been used as effective carriers for radiotracers given their high surface to area ratio.

Nanoparticles and Radiotracers: Imaging

Three main classes of radionuclides exist based on the type of decay exhibited: α, β, and γ radiation depicted in Figure 1. Alpha decay is the emission of a He^{+2} nucleus while beta particles can be further subdivided by their charge into two categories: positron (β^+, the antimatter of electrons) or high-energy electron (β^-). Lastly, gamma radiation is the emission of a high-energy photon. For the highest energy particles, the ejection of the charged decay particle occurs at ultra-relativistic speeds, affording another type of imaging modality known as Cerenkov Luminescence (CL), discussed later. The type of decay by the radiotracer determines the imaging method, contributes to the resolution of the images, and, in the case of therapy, the degree and range of cellular damage done at a given radiation dose.

Of utmost importance for designing a radiolabeling experiment for in vivo use is matching the biodistribution and pharmacokinetics of the NP with the intent of the radiotracing study. For NPs with fast clearance times, such as naked SNPs,[34] a radioisotope with a short half-life, such as ^{68}Ga ($t_{1/2}$ = 68m) is preferable for imaging in order to limit the dose of ionizing radiation to the subject. For therapy, longer lived radiolabeled NP are used, requiring high radiochemical stability to the NP, while also minimizing off target NP delivery minimizing the radiation dose to healthy tissue.

Imaging of NPs requires intrinsic particle properties that differ from the target tissue, such as a magnetic resonance contrast or a fluorophore. Radiolabeling utilizes the high-energy decay of a parent radionuclide as the imaging source. The amount of contrast agent necessary for nuclear medicine is magnitudes less than typical contrast concentrations for MR and CT. However, PET and SPECT have lower spatial resolution than these modalities with SPECT typically having the lowest due to collimator rejection to determine angle of incidence.[35] Radionuclides used for imaging typically have high specific activities such that picomolar (or even less) amounts of radiotracer are often used that usually do not induce any detectible effect or harm from the radiation to the organism. This is commonly referred to as the “radiotracer principle”.

Multimodal imaging is possible when NPs with already existing intrinsic imaging properties are functionalized with radionuclides e.g., IONPs labeled with a radiotracer allow for MR/PET imaging.[36] By combining modalities, a better image of the NP biodistribution can be determined without terminal studies.

Nanoparticle Radiolabeling

The type of radionuclide and NP chosen for imaging will determine the incorporation strategy into the NP. Traditional methods for radiolabeling a NP involves the attachment of a chelator such as 1,4,7,10-tetraazacyclododecane-1,4,7,10-tetraacetic acid (DOTA) or deferoxamine (DFO) for radiometal chelation,[37] or prosthetic groups such as tyrosine residues of proteins by using chloramine-t-oxidation (referred to as the IODOGEN

method)[31] to the NP surface for subsequent radiolabeling. Because of the wide use of chelators and prosthetic groups for labeling antibodies and peptides, these two methods are the main routes of NP radiolabeling.

Radionuclides can also be directly incorporated into the NP without using a chelator or prosthetic group as outlined in Figure 2. Three main methods are used for chelate-free radiolabeling: hot-plus-cold synthesis, ionic exchange, and cyclotron bombardment.[24] While radionuclide incorporation during synthesis typically results in stable in vivo constructs, the resulting generation of radioactive waste, longer radiolabeling times compared to other methods, and the necessity of the radionuclide to incorporate into the NP lattice without resulting in lattice mismatch are all limitations. Furthermore synthesis of the particle has to be much shorter than the decay of the radioisotope to preserve radiotracing functionality. Radiolabeling IONP,[38,39] SNP and silica-coated NPs,[40] and quantum dots involves pH dependent addition of the radiometal to the NP at elevated temperatures.[41] Chelator free radiolabeling of IONPs was reported through a 120°C incubation of radiometal salts in aqueous buffer for an hour.[38] In another example, ^{198}Au-NP were grown from cold AuNP precursors[42] while another method with ^{64}Cu alloyed AuNPs showed improved radiochemical stability compared to chelator and chelator free radiolabeling methods.[43] Lastly, NPs can also be radiolabeled through direct proton or neutron bombardment of the NP to produce the radionuclide in-situ, although this method requires an on-site cyclotron.[44] Unique methods of radiolabeling have also recently been shown with CNTs harboring ions within defects and were exploited for novel ^{225}Ac incorporation yielding a chelator free construct as depicted in Figure 3.[45] CNTs have served as a backbone for imaging moieties; however, pristine semiconducting single walled CNTs (SWCNTs) have IR optical properties[46], which are quenched by some direct CNT radiolabeling methods.[47]

PET Imaging

The two main nuclear imaging modalities are Positron Emission Tomography (PET) and Single Photon Emission Computed Tomography (SPECT), each offering unique capabilities. PET imaging is possible due to the annihilation of a positron emitted from a radionuclide with its matter counterpart, the electron. This annihilation releases energy in the form of two 511keV photons emitted at nearly 180°. These high-energy photons mostly pass through the body of the subject and are detected by a ring of detectors around the subject. Importantly, the more matter these photons pass through prior to reaching the detector, the greater the absorption, or attenuation, of the photons.[48] With the use of MR or CT in conjunction with PET, the attenuation of the photons can be corrected, allowing determination of quantitative standard uptake values (SUVs).[49] When a detector registers a signal, the instrument determines the coincident signal in the detector position opposing it (i.e. 180° away). This allows the instrument to determine a decay occurred somewhere between the two detectors. With annihilation time of flight corrections standard in modern instruments, resolution has been further improved. By collecting millions of events, a quantitative, whole-body image is reconstructed, as each coincidence detection corresponds to one radionuclide decay. Common radioisotopes for PET imaging include ^{11}C, ^{18}F, ^{64}Cu, ^{68}Ga, ^{82}Rb, ^{89}Zr, and ^{124}I. As each photon pair is directly related to a single decay, PET imaging is quantitative; thus

radiolabeled NPs can be imaged quantitatively to determine tumor uptake provided the radiotracer does not separate from the NP.

^{11}C ($t_{1/2}$ = 20m) is typically not used with NPs due to the extremely short half-life, although one study has shown feasibility. [^{11}C]methyl iodide was used to form covalent bonds with both carboxylic acid and amine functional groups bound to IONPs, which was subsequently used in vivo as a PET/MR contrast agent.[50] Likewise, ^{13}N ($t_{1/2}$ = 9.97m) required direct bombardment of Al_2O_3 NPs, thereby negating a radiolabeling step for use in vivo, allowing imaging out to 68 minutes.[44] The isotope ^{68}Ga ($t_{1/2}$ = 68m) offers a half-life just barely amenable for in vivo imaging of small, short-circulating NPs and has been used for both PET and Cerenkov imaging. PEGylated IONP have been radiolabeled and used for sentinel lymph node imaging, allowing PET/MR/CLI imaging.[51] Gold glucose-NPs (2–3 nm) with a neuropeptide attached were radiolabeled with ^{68}Ga to investigate blood-brain barrier (BBB) permeability. Attachment of a neuropeptide resulted nearly 3-fold increase in BBB permeability (0.020% ID/g) compared to non-targeted GNPs (0.0073% ID/g). However, such low uptake levels are quite difficult to discern using non-invasive PET, and only ex vivo tissue activity measurements showed convincing differences in uptake between control and targeted NPs.[52] The halogen ^{18}F ($t_{1/2}$ = 110m) is typically attached to NP via synthetic methods, and allows imaging out to 8 hours post-injection. An interesting alternative to synthetic methods involved using a proton beam to bombard TiO_2 NP resulting in the ^{18}O (p,n) ^{18}F reaction, providing a ^{18}F-intrinsically radiolabeled NP. Along with ^{18}F, ^{48}V ($t_{1/2}$ = 16d) was also produced via the ^{48}Ti(p,n) ^{48}V reaction, which may be an undesirable biproduct.[53] Another interesting route for ^{18}F labeling used a silicon–fluorine prosthetic group to conjugate ^{18}F to maleimide-containing AuNP.[54] 4-[^{18}F]fluorobenzyl-2-bromoacetamide ([^{18}F]FBBA) was used for radiolabeling precursor polymers, which were subsequently integrated into a polymeric NP using nanoprecipitation.[55]

If longer in vivo time points are desired, ^{64}Cu ($t_{1/2}$ = 12.7h) easily allows for imaging out to 48 hours. Recently, direct incorporation of a porphyrin into the polar head group of a lipid produced a novel chelating lipid that also self assembled. The authors showed that ^{64}Cu could be incorporated into the porphysomes with high serum stability to 48 hours. PET imaging of untargeted porphysomes in vivo was able to resolve margins of an orthotopic PC3 prostate cancer tumor in mice. Most importantly the radiolabeled porphysomes retained particle size, optical properties, and had nearly identical biological half lives to cold liposomes showing radiolabeling did not significantly change the particle as seen in many other examples.[56] In another study, imaging of orthotopic lung tumors was achieved using chelator-free [^{64}Cu]Cu nanoclusters including BSA and luteinizing hormone releasing hormone (LHRH) as a targeting agent. The authors utilized a one-pot synthesis to incorporate ^{64}Cu as a building block in the BSA nanocluster in lieu of radiolabeling via traditional DOTA or 1,4,8,11-tetraazacyclotetradecane-1,4,8,11-tetraacetic acid (TETA) chelators. The inclusion of LHRH on the ^{64}Cu BSA nanocluster led to a nearly four-fold increase in delivery to the lung though greater uptake was also seen in both the liver and the kidney based on 4 hour biodistribution activity counts in Figure 4.[57] Previous work by others highlighted a similar approach for CT imaging and radiosensitization through the direct incorporation of cold Au within a glutathione shell.[58] Imaging the progression of atherosclerosis was shown in a spontaneous $ApoE^{-/-}$ mouse model using a ^{64}Cu-vMIP-II-

comb NP. The 15.8nm NP comb contained approximately 4 viral macrophage protein II (vMIP-II) peptides and 70 DOTA chelators per NP with the goal of correlating uptake with macrophage infiltration as vMIP-II is expressed on macrophages. In the spontaneous atherosclerosis mouse model, higher uptake of the ^{64}Cu-vMIP-II-comb NPs were seen between 20 and 37 weeks in the ApoE$^{-/-}$ mice suggesting increasing macrophage infiltration and progression of disease. Histology of the artery sections confirmed higher macrophage presence between 20 and 37 weeks. In a vascular injury model the ^{64}Cu-vMIP-II-comb NPs had a higher uptake in the wire injured artery compared to a sham operation on the opposing femoral artery.[59]

The longest-lived PET isotopes commonly used for NP imaging are ^{89}Zr ($t_{1/2}$ = 78.4h) and ^{124}I ($t_{1/2}$ = 4.18d). Mesoporous SNPs were labeled with DFO and shown to be stable in vivo, with uptake in the RES. While the DFO is commonly used for ^{89}Zr radiolabeling, recent work with SNP[40,60] has shown that by incubating particles with oxophilic radionuclides at temperatures >70°C, chelate-free radiolabeling of numerous isotopes can be achieved with SNP. This method is also effective for radiolabeling silica-coated IONP with ^{68}Ga, showing the versatility of the method.[39] An analogous method for radiolabeling the clinically approved IONP Feraheme, coined heat induced radiolabeling (HIR) by the authors, was demonstrated and may be a route for radiolabeling other metal oxide NPs with oxophilic tracers.[38] Omitting the IONP core, chelator free loading of ^{89}Zr was also observed using various molecular weight dextran NPs for PET/CT imaging of lymph node drainage as well as Cerenkov guided tumor resection.[61] ^{89}Zr was also loaded into high-density liposome (HDL) for the tracking of tumor-associated macrophages (TAMs) in a murine breast cancer model. Using DFO as a chelation agent, ^{89}Zr was attached to phospholipid and ApoA HDL and tracked in vivo over 24hr in mice with 4T1 tumors.[62] Another approach used HIR to load ^{89}Zr into the iron oxide core of Feraheme for monocyte tracking.[63] The authors were able to track the fast and slow NP uptake processes for the first time using PET-derived PK. Of note, the slow process was driven by trafficking of NP loaded monocytes, giving insight to monocyte movement in vivo.

In another example, a ScFv anti-MET antibody fragment was dimerized to produce a cys-diabody and site specifically radiolabeled with ^{89}Zr using a DFO maleimide chelator. The anti-MET cys-diabody was rapidly screened from a phage display library to target non-small lung cell carcinoma, and other cancers that overexpress MET. MET, the receptor of hepatocyte growth factor has roles in tumorigenesis and drug resistance. The diabody design allowed for rapid imaging of tumors while maintaining a higher tumor to blood signal than a larger minibody which has a longer serum persistence. Furthermore the targeting of MET allows for the identification of drug resistant tumors as well as potential therapy.[64] One particle already in clinical trials is ^{124}I-radiolabeled ultra small C dots targeted with RGD peptide and tagged with an optical dye, Cy5.[65] Integrin-expressing tumors were delineated non-invasively via PET imaging with the^{124}I-C dots, while the Cy5 dye allows surgical guidance for tumor resection.

SPECT Imaging

SPECT imaging takes advantage of the emission of a high-energy photon (gamma) from the nucleus of a radionuclide. Collimators designed to detect a specific range of photon energies register a signal upon photon detection. Typically, two-detector systems located opposite of each other (or in rare cases perpendicular, e.g. for cardiac imaging) are used that acquire images through rotating from multiple angles around the field of view, which are then reconstructed into 3-dimensional images. Typical full-width half-maximum resolutions of SPECT and PET systems in preclinical machines are on the order of ~10mm and ~5mm respectively, which are an order of magnitude worse than CT and MRI.[66] Using newer multi-pinhole collimators for SPECT together with sophisticated reconstruction algorithms can however improve the resolution of SPECT significantly. The ubiquity of the generator-produced SPECT tracer ^{99m}Tc allows nuclear imaging in institutes without easy access to cyclotrons. ^{99m}Tc ($t_{1/2}$ = 6h) allows SPECT imaging typically out to one day post-injection, and has mature radiochemistry as the most widely used medical radiotracer. ^{99m}Tc has been attached to IONP,[67–69] silver NP (AgNP),[70] AuNP,[71] and SNP[67,72] among others. Other ^{99m}Tc tracers include a FDA approved formulation of ^{99m}Tc-sulfur nanocolloid filtered <100nm for imaging of sentinel lymph nodes (SLN) in prostate cancer.[73] SLN mapping using filtered ^{99m}Tc-sulfur nanocolloid was found to be comparable to the ^{99m}Tc-Nanocoll human serum albumin formulation also under clinical investigation. A more in depth coverage of SLN mapping with ultra small SNPs can be found in this review.[74]

For longer imaging studies, ^{111}In, ^{67}Ga, and various iodine species are used. ^{67}Ga ($t_{1/2}$ = 2.2d) and ^{111}In ($t_{1/2}$ = 2.8d) have been used to radiolabel NP via both chelate-free methods[40,41] as well as a diethylenetriamine-pentaacetic acid (DTPA) chelator.[75] D-Glucosamine coated micelles were radiolabeled with ^{111}In using a DTPA chelator and showed 2.62% Id/g in a human epithelial carcinoma A-431 xenograft model at 24 hours post-injection, allowing tumor delineation. Visualization of cell death by both nuclear and optical techniques was achieved using ^{111}In-labeled annexin A5-conjugated core-cross-linked polymeric micelles in vivo via both SPECT and fluorescence.[76] To investigate the whole body biodistribution of nanotubes, SWCNTs were radiolabeled with either ^{86}Y ($t_{1/2}$ = 14.7h) or ^{111}In in mouse models showing biodistribution and clearance in kidney, liver, spleen, and bone over 24 hours i.v. and i.p.[47] Further work developed a novel method to produce lysine modified SWCNTs yielding a more favorable handle for chelator attachment. Lysine modified SWCNTs showed improved biodistribution properties of ^{111}In radiolabeled DOTA conjugated lysine SWCNTs[77].

A recent report on highly specific SPECT/CT imaging used an ^{111}In anti-PSMA nanobody for targeted imaging. By combining the rapid clearance of the nanobody alongside the specificity for PSMA expressing prostate cancer cell lines, radiotracing with the SPECT emitter ^{111}In showed high uptake in PSMA positive tumors, with no appreciable uptake in PSMA negative tumors present in the same xenograft model. Radiolabeling was done using DTPA in a one-step room temperature synthesis.[17]

Some isotopes emit therapeutic electrons but also gamma photons, allowing both therapy and SPECT imaging with the same radioisotope. Examples such as ^{131}I ($t_{1/2}$ = 8d),

and ^{177}Lu ($t_{1/2}$ = 6.7d) will be discussed in the theranostics section. Non-therapeutic uses of ^{131}I are often used as ^{124}I analogs in pre-clinical studies due to their much lower cost. ^{131}I is radiolabeled via identical methods as ^{124}I (and other iodine radioisotopes). Lastly, with a half-life of 50 days, ^{125}I labeled albumin and transferrin was used to investigate the protein corona of ^{59}Fe-SPIOs.[78]

Cerenkov Imaging

A relatively recent medical imaging modality that utilizes certain radiotracers is Cerenkov luminescence (CL). CL occurs when a charged particle travels faster than the phase velocity of light in a medium. CL was first described in the 1930's by Vavilov and a member of his lab, Pavel Cherenkov. Cherenkov, along with fellow lab members Frank and Tamm, shared the 1958 Nobel Prize in physics for their discovery. CL is emitted in the same direction as the traveling charged particle, with an angle of distribution that is dependent on the velocity of the charged particle and the refractive index of the medium through which the particle is passing. Therefore, knowing this angle allows the velocity of the particle to be determined and this relationship was used for high-energy particle characterization. However, it was not until 2009 that CL was used for in vivo imaging when Robertson *et al.* showed that the positron emitters ^{89}Zr and ^{18}F emit CL and could be used for pre-clinical imaging. The authors coined the technique Cerenkov Luminescence Imaging, or CLI.[79] Additional radionuclides were subsequently found to produce CL in preclinical studies yielding a broad collection of α, β^+, and β^- emitting nuclides including ^{18}F, ^{64}Cu, ^{89}Zr, ^{90}Y, ^{68}Ga, ^{124}I, ^{131}I, ^{177}Lu, and ^{225}Ac. These cover a wide range of energies from ^{177}Lu (E_{Max}=0.497MeV) to ^{225}Ac (E_{Max}=5.94MeV). CL importantly enables the imaging of β^- radionuclide decay, which PET and SPECT imaging techniques are unable to detect directly. CL is characterized by an emission intensity of $1/\lambda^2$ in the visible region and as such often described as a blue glow.

Quickly after CLI was first described, quantum dots were combined with CL, with the resulting phenomenon coined Cerenkov Radiation Energy Transfer (CRET).[80] Additional studies demonstrated that CL from ^{131}I could excite QD655/QD705/QD800 in vitro and in vivo.[81] Subsequently, ^{64}Cu doped AuNP nanoclusters were used in vivo to track U87MG glioblastoma tumors with CL, PET and NIR methods producing 15.2% ID/g uptake of the nanoclusters in tumors after 24 h.[82] Building on this work, the production of an self illuminating QD using a ^{64}Cu doped CdSe/ZnS QD was completed.[83] In vivo, the QD was shown to have a 12.7% ID/g uptake in their U87MG glioblastoma xenograft model. Recently, ^{198}Au seeded NPs with varying aspect ratios were utilized to show via CL the influence of shape on biodistribution.[84] Pegylated nanospheres, nanocages, nanorods, and nanodisks were tested in vivo using CL and confirmed via gamma counting differences in biodistribution up to 24h post injection. Figure 5 shows the notable differences in biodistribution of particles with varying aspect ratios at 1 and 24 hours post injection.

More sophisticated, biologically inspired, and activatable probes were described by Thorek et al. to produce secondary Cerenkov-induced fluorescence imaging or SCIFI.[85] Fluorescein was tethered to a matrix metallopeptidase-2 (MMP-2) cleavable sequence on an AuNP. With ^{18}FDG as the CL source, uncleaved fluorescein was quenched by the AuNP and only

available for SCIFI once MMP-2 activity liberated fluorescein from the AuNP quencher. SCIFI was shown to increase the signal to noise ratio of CL six-fold compared to traditional external fluorescence techniques due to entirely internal excitation from the CL. Proximal conversion of CL to any fluorophore based upon enzymatic activity is key to biorelevant signal amplification.

Multimodal Imaging through Optically Active NPs

Integration of multiple detection methods into a single system, such as fluorescence, SPECT, PET, CT, or MR scanning, has fostered the development of radiolabeled multimodal NPs. Multimodal imaging relies on the intrinsic property of the NP or an agent attached to the particle other than the radionuclide. Several metal NPs including Fe, Au, Zn, and Ti elements have been chosen for their multimodal imaging and therapeutic properties. These metal NPs depending on their intrinsic property can be used as MR (Fe NP), photoacoustic, radiosensitizers (ZnO or TiO2 NPs), and hyperthermal agents (AuNPs)[86]. Choosing the right radiotracer with a reportable NP can yield advanced multimodal imaging as well as therapeutic potential.

Traditional fluorescence techniques have also been employed with multimodal radiotracers yielding dual labeled NPs. C dots, as previously mentioned, have been investigated in the clinic using a ^{124}I label for PET and Cy5 for optical imaging and resection of $\alpha_v\beta_3$ integrin tumors[31]. ZnO NPs have also been used as dual fluorescent PET imaging agents with ^{64}Cu.[87] Quantum dots have emerged as a leading NP for fluorescence imaging due to their specific emission bandwidth, quantum efficiency, and resistance to photobleaching. Newer generations of QDs made from biocompatible materials have been made with chelated radionuclides for PET/fluorescence imaging. A chelator free Cu-In-Se QD was recently prepared for in vivo SPECT/fluorescence imaging using ^{111}In directly between the core and shell of the QD. Furthermore material biocompatibility was enhanced through the use of a multidentate zwitterionic polymer surface showing high uptake into COLO-205 tumor bearing mice via SPECT/CT and fluorescence imaging 6 hours post injection.[88]

Super paramagnetic IONPs (SPION) have been mostly used as MR contrast agents but can also serve as platform for multimodal imaging. Combining MR agents with radiotracers takes advantage of the best of each imaging modality, such as quantitative results from PET and morphological T1 or T2 weighted contrast in MRI. A recent review on engineering radiolabeled IONPs covers numerous examples of dual mode imaging.[89] Traditional contrast agents involve chelated paramagnetic gadolinium for T1 contrast adjustment, while SPIONs have been used for T2 contrast, but are not widely approved in the US. MR contrast agents rely on altering the T1 or T2 relaxivities for a feature of interest. Recent interest in combining MR with radiotracers has led to the use of SPION as the MR NP of choice. Metal oxides, such as TiO_2, have been widely used as purification media in Ge generators, but are not limited to chromatographic uses. The intrinsic labeling of Ge to a metal oxide surface represents an area of recent interest for NPs and radiotracers as well as exploiting magnetic properties imbued by SPION. Recently ^{69}Ge was intrinsically radiolabeled onto an iron oxide NP for multimodal SPION radiotracing for PET/MR.[90] Using a PEGylated ^{69}Ge SPION, in vivo uptake in the liver via PET as well as T_2^*-MRI was seen with no observable

accumulation in the kidney. Furthermore these NP were injected into murine foot pads to show lymph node drainage over 20 hours. Chelator free radiolabeling of PEG functionalized, silica coated iron oxide nanorods revealed high radiochemical stability comparable to chelator analogues produced. It was also shown that the type of chelator coated affected the T_1 and T_2 relaxivity of the iron oxide nanorods.[39] Intrinsic multimodal imaging for MR/radiotracing was also recently achieved through direct synthesis of ^{59}Fe SPION NPs from cold precursor seeds. Through direct incorporation of the radionuclide in the synthesis, minimal changes to MR relaxivity properties were observed.[78] Traditional methods for multimodal imaging involve surface conjugation or core shell modification to add multimodal imaging functionality. In a recent report, a novel radiolabeling approach combined reactive thiols for AuNP targeting as well as a flexible PEG linker and chelator to secure $[^{99m}Tc(CO)_3]^+$ to the particle surface. Using both core shell and dumbbell synthesis methods for Au-Fe_3O_4 NPs, the attached novel linkers produced a multimodal NP for SPECT imaging. By altering the type of particle produced, the dumbbell-like AuNPs had high colloidal stability that did not require surface conjugation.[91]

PET/MR multimodal imaging was achieved by using ^{68}Ga chelator-free silica coated nanorods.[39] Increased T_1 and T_2 relaxivities were observed with PEGylated, chelator free nanorods with subsequently high radiochemical stability for ^{68}Ga in serum over 3 hours for chelated and chelator free radiolabeled nanorods. Recently the synthesis of a GdF_3, ^{90}Y doped NP for MR/CLI was reported. Using high morphology and size control during synthesis the authors produced rhomboid nanoplates 15.5±1.3nm in size that were further surface modified with nitrosonium tetrafluoroborate and finally a water soluble polymer to enable aqueous compatibility. The GdF_3:^{90}Y/Y nanoplates produced both high CL as well as MR contrast agent properties highlighting a multimodal bottom up synthesis method.[92]

Many of the NPs reported in radiotracing studies are not FDA approved, and as such require long-term safety and efficacy studies before they can be used as imaging agents in patients. One approach is to use already available and FDA-approved NPs as platforms for drug delivery and radiolabeling. On such example is the FDA approved iron oxide NP Ferumoxytol which was utilized as a drug delivery vehicle without significant modification to the NP. Here, Ferumoxytol was used as an environment sensitive nanophore based on drug release from the dextran particle coating. Loading the NP with a ^{131}I labeled HSP90 inhibitor, the iron oxide NP served not only as a T2 contrast agent sensitive to the concentration of drug released, but radiolabeling allowed biodistribution studies as well. This combination showed enhanced tumor delivery compared to radiolabeled drug alone.[33] In a similar fashion, Ferumoxytol was used as a MR NP platform for ^{89}Zr radiolabeling. Using well-known EDC coupling of DFO to free carboxyl groups on the dextran shell, the authors were able to radiolabel without alteration in particle size and serum stability to 24 hours. These radiolabeled Ferumoxytol particles were used in high resolution PET/MR imaging studies for the detection of sentinel lymph nodes and the monitoring lymph node drainage.

Multimodal imaging with radiolabeled NPs give researchers and hopefully in the near future clinicians the power to move between imaging modalities, where each method yields information about the biology of the environment around the NP. Current advances report

hexamodal imaging with single NP systems highlight the sophistication of NP design possible.[93] Figure 6 shows the breadth in information extracted from a hexamodal system, while also revealing the bias one particular imaging modality may provide. Hexamodal NPs also reveal the complexity required to produce a translatable particle, making it harder to bring though the clinic for each imaging modality. Here single imaging modality NPs can be sufficient for clinical development as seen by the advancement of C dots in the clinic. While these methods rely heavily on imaging and are not mentioned as therapeutic agents, radiolabeling with therapeutic isotopes such as ^{90}Y, ^{131}I, ^{177}Lu, and ^{225}Ac opens the ability for imaging agents to become radionanomedicines as well.

Theranostics

Therapy utilizing radiation traditionally can be separated into external, internal, and systemic radiation therapy. External radiation therapy utilizes x-rays, electron, or proton beams focused into a region of interest. Advancements such as Intensity Modulated Radiation Therapy (IMRT) have allowed clinicians to deliver higher radiation doses to patents with hyperfractionation, the administration of a total dose of radiation broken into several shorter daily doses. Alternatively internal radiation, or brachytherapy, uses implantation of radioactive seeds, such as ^{90}Y microspheres to deliver highly localized doses to a tumor. As a result, even higher radiation doses can be delivered to patients using brachytherapy with fewer side effects than external radiation therapy.[94] Lastly endoradiotherapy requires delivery of a radiotracer via oral or intravenous methods with the intent of targeting a tumor.

NPs loaded with therapeutic isotopes represent a form of systemic radiation therapy, and given the high specific activity of radionuclides, NPs could be loaded with levels of therapeutic radionuclides serving as “nano seeds” as in brachytherapy. As NPs are significantly smaller than implanted seeds, NPs will have higher diffusion speeds compared to micron or millimeter sized seeds. Thus for a successful theranostic NP, the NP needs to be engineered for high radiochemical stability, tumor co-localization and distribution within a tumor while avoiding non-tumor tissue. Radiolabeled NPs with these properties could provide greater coverage than current brachytherapy to the target tumor. A clear disadvantage of this method is the potential escape of therapeutic radiolabeled NPs from the target tumor due to their smaller size than current seeds. Previous issues with traditional brachytherapy have involved particle transport outside of the tumor, as well as limited delivery throughout a tumor despite the mm long path length of many β-emitting radionuclides. Finding the right combination of therapeutic radionuclide with tumor targeting and retention mechanism while avoiding the MPS could allow imaging agents to become theranostics candidates for the clinic.[95] Addressing NP migration from tumors, a laminin targeted β-emitting ^{198}AuNP was injected intratumorally and was highly retained in the tumor post injection, resulting in static PC3 prostate tumor volume in vivo as seen in Figure 7.[42] While NPs can be retained in a tumor and subsequently reduce tumor burden, maintaining the activity with the NP is an additional concern. Serum stability tests are often done, and in the case of radionuclides with decay daughters, additional sequestration design is necessary for the NP.

Traditionally, α-emitting radionuclides such as ^{225}Ac have been attached through chelation and considered ideal therapeutic radionuclides given their high Linear Energy Transfer (LET) and single cell path length before annihilation (50–100μm). β-emitting radionuclides with lower LETs and greater annihilation distances of several cells (typically 0.2–12mm) provide a larger and tortuous radiative dose volume. While α-emitters are considered better therapeutic agents, ^{225}Ac daughters are an off target concern as chelation is insufficient during decay to retain daughters due to the recoil from the heavy alpha particle leaving the nucleus. Furthermore with a long ($t_{1/2}$=10d) half-life, an encapsulation strategy would be favored. A core-shell NP was designed to sequester the daughters inside the NP without loss of α-emitting dose, while affording the NP multimodal imaging properties.[96] A $\{La_{0.5}Gd_{0.5}\}PO_4$ core was used to house the ^{225}Ac, a $GdPO_4$ layer to retain the majority of the decay chain daughters, and lastly the Au shell facilitates attachment of targeting agents. The authors note that the $GdPO_4$ shell could be used for MR contrast, and the Au surface could be used for targeting ligand attachment. The produced NP was capable of sequestering 88% of the ^{221}Fr decay daughter while reducing the energy of the α-particles emitted by only 0.2%. Furthermore in vivo biodistribution of the untargeted NP was predominantly in the liver with 2.8% of the injected dose migrating as ^{213}Bi to the kidneys after one hour compared to 10% with the $LaPO_4$ core particles highlighting retention of daughter radionuclides within the NP. Lastly the authors conjugated a mAb targeting thrombomodulin receptors in the lung to the $\{La_{0.5}Gd_{0.5}\}(^{225}Ac)PO_4$@$GdPO_4$@Au NP. Addition of the mAb drastically changed the biodistribution resulting in high uptake of the NP-mAb combination to the lung.[96] Another strategy for ^{225}Ac incorporation involved placement inside ultrashort SWCNT (US-tubes). US-tubes were prepared containing surface defects that would allow internalization of an ion. The authors tested loading conditions for $^{225}Ac^{3+}$ and Gd^{3+} and challenged internalization with heat, time and serum incubation. The authors were able to show two distinct populations of $^{225}Ac^{3+}$ ions existed with the US-tubes, with one population internalized such that heat, time, and serum challenges could not liberate the radionuclide.[45]

Theranostic agents utilizing SPECT tracers such as ^{131}I and ^{177}Lu allow imaging and therapy without the consideration of radioactive daughters as in the case of ^{225}Ac. ^{131}I is commonly used for thyroid therapy. With a 50 day half-life, ^{125}I is useful for long-term biological studies and brachytherapy. While less explored compared with iodine species, ^{177}Lu has been attached to gold NPs for imaging and therapy in tumor-bearing mice.[97]

In a recent study, radiolabeled ^{177}Lu AuNPs with RGD targeting showed the highest tumor delivery compared to non-RGD as well as RGD ^{177}Lu controls respectively. Most importantly the ^{177}Lu AuNP RGD construct delivered a 63.8 Gy dose to the tumor based on uptake, highlighting the potential therapeutic capacity for radiolabeled NPs for endoradiotherapy. This increased uptake was shown both in vitro with reduced cell proliferation as well as in vivo with significantly reduced tumor volume. Biodistribution within the tumor was also imaged and showed more homogeneous distribution through the tumor, leading to fewer necrotic regions when compared against ^{177}Lu-RGD, ^{177}Lu-AuNP and control ^{18}FDG administration.[97] ^{177}Lu has also been loaded with high stability into a lipid-calcium-phosphate (LCP) delivery platform for theranosis.[98] Intravenous injections

of ^{177}Lu-LCP into mice with UMUC3 or human H460 xenograft tumors showed tumor uptake both by SPECT/CT as well as CL while free ^{177}Lu resided in the spine. Single injections of 200–250uCi of ^{177}Lu-LCP compared to free ^{177}Lu showed reduced tumor volumes. Toxicity was seen with free ^{177}Lu resulting in immunocompromised mice, while ^{177}Lu-LCP did not reveal renal or hepatotoxicity yet presented decreased white blood cells and platelets.

While certain radionuclides can be used for imaging as well as radiation therapy, the radionuclide does not have to be the therapeutic agent. A recent report showed the use of mPEG-Grafted Poly(L-Lysine) stabilized AuNPs for SPECT/CT using ^{99m}Tc. The addition of the mPEG Poly(L-Lysine) yielded not only NP stability but also served as a biocompatible scaffold for further particle modification. In vivo results showed long circulation times in the blood, with minimal uptake in major organs with uptake at sites of inflammation. The Au core of the NPs was further shown after delivery to be useful for thermal ablation therapy conferring theranostic capability.[99] Another method utilized CNTs as a scaffold for the radiotracer ^{99m}Tc, alongside fluorophores AF488/647, a folic acid targeting ligand, and the anticancer drug methotrexate. The multimodal agent had superior methotrexate release and was able to rapidly inhibit growth in a chemically induced 7,12-Dimethylbenz[α]anthracene tumor model.[100]

Conclusions and outlook

NPs have gained tremendous interest as tools for biomedical applications in recent years with increasing use of multimodal components. As NP complexity built on the knowledge of liposome manufacture, radiotracers could be added to image the delivery of the particle to the intended target. PET and SPECT imaging methods have matured while new modalities such as CL have emerged enabling a wider array of radionuclides for imaging. In the case of CL, radionuclides used previously for radiation therapy, such as β^- emitting ^{90}Y, can now be imaged. Convergence of radiolabeling with the cornucopia of NPs for imaging and therapy has resulted in many particles capable of multimodal imaging. With most recent examples capable of hexamodal imaging, next generation NP design needs not another increasingly complex imaging agent but rather increased sophistication in target specificity, feature margin, and biologically relevant signal amplification. Also, the applicability of many nanoparticle constructs has to be critically reviewed. Many of the NP platforms described in this review image and potentially treat tumors that are well established but were not designed to address smaller tumors lacking vasculature or even single circulating tumor cells. By engineering radiolabeled NPs with amplification techniques, single cells of interest could become viable targets for imaging and therapy.

Acknowledgments

We acknowledge funding from the National Institutes of Health (NIH) R01EB014944 and R01CA183953 and National Science Foundation Integrative Graduate Education and Research Traineeship Grant (NSF) IGERT 0965983.

References

1. Harmsen S, et al. Surface-enhanced resonance Raman scattering nanostars for high-precision cancer imaging. Sci Transl Med. 2015; 7:271ra7.
2. Lipinski CA, Lombardo F, Dominy BW, Feeney PJ. Experimental and computational approaches to estimate solubility and permeability in drug discovery and development settings. Adv Drug Deliv Rev. 2001; 46:3–26. [PubMed: 11259830]
3. Grimm J, Scheinberg Da. Will Nanotechnology Influence Targeted Cancer Therapy? Semin Radiat Oncol. 2011; 21:80–87. [PubMed: 21356476]
4. Lukyanov AN, Elbayoumi Ta, Chakilam AR, Torchilin VP. Tumor-targeted liposomes: Doxorubicin-loaded long-circulating liposomes modified with anti-cancer antibody. J Control Release. 2004; 100:135–144. [PubMed: 15491817]
5. Torchilin VP. Targeted polymeric micelles for delivery of poorly soluble drugs. Cell Mol Life Sci. 2004; 61:2549–2559. [PubMed: 15526161]
6. Discher BM, et al. Polymersomes: tough vesicles made from diblock copolymers. Science. 1999; 284:1143–1146. [PubMed: 10325219]
7. Duncan R, Izzo L. Dendrimer biocompatibility and toxicity. Adv Drug Deliv Rev. 2005; 57:2215–2237. [PubMed: 16297497]
8. Liu Z, Tabakman S, Welsher K, Dai H. Carbon nanotubes in biology and medicine: In vitro and in vivo detection, imaging and drug delivery. Nano Res. 2009; 2:85–120. [PubMed: 20174481]
9. Stöber W, Fink A, Bohn E. Controlled growth of monodisperse silica spheres in the micron size range. J Colloid Interface Sci. 1968; 26:62–69.
10. Israelachvili, JN. Intermolecular and Surface Forces Intermolecular and Surface Forces. Elsevier; 2011.
11. Schroeder A, et al. Treating metastatic cancer with nanotechnology. Nat Rev Cancer. 2011; 12:39–50. [PubMed: 22193407]
12. Gratton, SEa, et al. The effect of particle design on cellular internalization pathways. Proc Natl Acad Sci U S A. 2008; 105:11613–11618. [PubMed: 18697944]
13. Kolhar P, et al. Using shape effects to target antibody-coated nanoparticles to lung and brain endothelium. Proc Natl Acad Sci U S A. 2013; 110:10753–8. [PubMed: 23754411]
14. Ruggiero A, et al. Paradoxical glomerular filtration of carbon nanotubes. Proc Natl Acad Sci U S A. 2010; 107:12369–12374. [PubMed: 20566862]
15. Roode LE, et al. Subtumoral analysis of PRINT nanoparticle distribution reveals targeting variation based on cellular and particle properties. Nanomedicine. 2016; :1–10. DOI: 10.1016/j.nano.2015.12.382
16. Maeda H, Wu J, Sawa T, Matsumura Y, Hori K. Tumor vascular permeability and the EPR effect in macromolecular therapeutics: A review. J Control Release. 2000; 65:271–284. [PubMed: 10699287]
17. Hansen AE, et al. Positron Emission Tomography Based Elucidation of the Enhanced Permeability and Retention Effect in Dogs with Cancer Using Copper-64 Liposomes. 2015
18. Lammers T, et al. Theranostic USPIO-loaded microbubbles for mediating and monitoring blood-brain barrier permeation. Adv Funct Mater. 2015; 25:36–43. [PubMed: 25729344]
19. Werner ME, et al. Folate-targeted nanoparticle delivery of chemo- and radiotherapeutics for the treatment of ovarian cancer peritoneal metastasis. Biomaterials. 2011; 32:8548–8554. [PubMed: 21843904]
20. Pressly ED, Pierce Ra, Connal La, Hawker CJ, Liu Y. Nanoparticle PET/CT imaging of natriuretic peptide clearance receptor in prostate cancer. Bioconjug Chem. 2013; 24:196–204. [PubMed: 23272904]
21. Sá LTM, et al. Development of nanoaptamers using a mesoporous silica model labeled with 99mTc for cancer targeting. Oncology. 2012; 82:213–217. [PubMed: 22508189]
22. Zhang M-Z, Yu R-N, Chen J, Ma Z-Y, Zhao Y-D. Targeted quantum dots fluorescence probes functionalized with aptamer and peptide for transferrin receptor on tumor cells. Nanotechnology. 2012; 23:485104. [PubMed: 23138109]

23. Karmani L, et al. Antibody-functionalized nanoparticles for imaging cancer: Influence of conjugation to gold nanoparticles on the biodistribution of 89Zr-labeled cetuximab in mice. Contrast Media Mol Imaging. 2013; 8:402–408. [PubMed: 23740810]
24. Goel S, Chen F, Ehlerding EB, Cai W. Intrinsically Radiolabeled Nanoparticles: An Emerging Paradigm. Small. 2014; :3825–3830. DOI: 10.1002/smll.201401048 [PubMed: 24978934]
25. Owens DE, Peppas Na. Opsonization, biodistribution, and pharmacokinetics of polymeric nanoparticles. Int J Pharm. 2006; 307:93–102. [PubMed: 16303268]
26. Rodriguez PL, et al. Minimal 'Self' peptides that inhibit phagocytic clearance and enhance delivery of nanoparticles. Science. 2013; 339:971–5. [PubMed: 23430657]
27. Beningo, Ka; Wang, Y. Fc-receptor-mediated phagocytosis is regulated by mechanical properties of the target. J Cell Sci. 2002; 115:849–856. [PubMed: 11865040]
28. Sosale NG, et al. Cell rigidity and shape override CD47's 'self' -signaling in phagocytosis by hyperactivating myosin-II. Blood. 2015; 125:542–552. [PubMed: 25411427]
29. MORGAN JR, et al. Localisation of experimental staphylococcal abscesses by 99MTC-technetium-labelled liposomes. J Med Microbiol. 1981; 14:213–217. [PubMed: 7230253]
30. Ow H, et al. Bright and Stable Core – Shell Fluorescent Silica Nanoparticles. Nano. 2005; doi: 10.1021/nl0482478
31. Benezra M, et al. Multimodal silica nanoparticles are effective cancer-targeted probes in a model of human melanoma. J Clin Invest. 2011; 121:2768–2780. [PubMed: 21670497]
32. Kircher MF, et al. A brain tumor molecular imaging strategy using a new triple-modality MRI-photoacoustic-Raman nanoparticle. Nat Med. 2012; 18:829–834. [PubMed: 22504484]
33. Kaittanis C, et al. Environment-responsive nanophores for therapy and treatment monitoring via molecular MRI quenching. Nat Commun. 2014; 5:3384. [PubMed: 24594970]
34. Van Schooneveld MM, et al. Improved biocompatibility and pharmacokinetics of silica nanoparticles by means of a lipid coating: A multimodality investigation. Nano Lett. 2008; 8:2517–2525. [PubMed: 18624389]
35. Rahmim A, Zaidi H. PET versus SPECT: strengths, limitations and challenges. Nucl Med Commun. 2008; 29:193–207. [PubMed: 18349789]
36. Thorek DLJ, et al. Non-invasive mapping of deep-tissue lymph nodes in live animals using a multimodal PET/MRI nanoparticle. Nat Commun. 2014; 5:3097. [PubMed: 24445347]
37. Zeglis BM, Houghton JL, Evans MJ, Viola-Villegas N, Lewis JS. Underscoring the influence of inorganic chemistry on nuclear imaging with radiometals. Inorg Chem. 2014; 53:1880–1899. [PubMed: 24313747]
38. Boros E, Bowen AM, Josephson L, Holland JP. Chelate-free metal ion binding and heat-induced radiolabeling of iron oxide nanoparticles. Chem Sci. 2015; 6:225–236.
39. Burke BP, et al. Chelator free gallium-68 radiolabelling of silica coated iron oxide nanorods via surface interactions: evaluation as multimodal PET/MR liver imaging agents. Nanoscale. 2015; doi: 10.1039/C5NR02753E
40. Shaffer TM, et al. Silica Nanoparticles as Substrates for Chelator-free Labeling of Oxophilic Radioisotopes. Nano Lett. 2015; 15:864–868. [PubMed: 25559467]
41. Zeng J, et al. In situ 111In-doping for achieving biocompatible and non-leachable 111In-labeled Fe3O4 nanoparticles. Chem Commun. 2014; 50:2170–2172.
42. Shukla R, et al. Laminin receptor specific therapeutic gold nanoparticles (198AuNP-EGCg) show efficacy in treating prostate cancer. Proc Natl Acad Sci. 2012; 109:12426–12431. [PubMed: 22802668]
43. Zhao Y, et al. Copper-64-alloyed gold nanoparticles for cancer imaging: Improved radiolabel stability and diagnostic accuracy. Angew Chemie - Int Ed. 2014; 53:156–159.
44. Pérez-Campaña C, et al. Biodistribution of Different Sized Nanoparticles Assessed by Positron Emission Tomography: A General Strategy for Direct Activation of Metal Oxide Particles. ACS Nano. 2013; 7:3498–3505. [PubMed: 23473535]
45. Matson ML, et al. Encapsulation of Alpha-Particle-Emitting 225Ac3+ Ions Within Carbon Nanotubes. J Nucl Med. 2015; 56:897–900. [PubMed: 25931476]

46. Bachilo SM, et al. Structure-assigned optical spectra of single-walled carbon nanotubes. Science. 2002; 298:2361–6. [PubMed: 12459549]
47. McDevitt MR, et al. PET imaging of soluble yttrium-86-labeled carbon nanotubes in mice. PLoS One. 2007; 2
48. Schulz V, et al. Automatic, three-segment, MR-based attenuation correction for whole-body PET/MR data. Eur J Nucl Med Mol Imaging. 2011; 38:138–152. [PubMed: 20922522]
49. Wiesmüller M, et al. Comparison of lesion detection and quantitation of tracer uptake between PET from a simultaneously acquiring whole-body PET/MR hybrid scanner and PET from PET/CT. Eur J Nucl Med Mol Imaging. 2013; 40:12–21. [PubMed: 23053323]
50. Sharma R, et al. Carbon-11 radiolabeling of iron-oxide nanoparticles for dual-modality PET/MR imaging. Nanoscale. 2013; 5:7476–83. [PubMed: 23832243]
51. Madru R, et al. (68)Ga-labeled superparamagnetic iron oxide nanoparticles (SPIONs) for multi-modality PET/MR/Cherenkov luminescence imaging of sentinel lymph nodes. Am J Nucl Med Mol Imaging. 2013; 4:60–9. [PubMed: 24380046]
52. Frigell J, García I, Gómez-Vallejo V, Llop J, Penadés S. 68Ga-labeled gold glyconanoparticles for exploring blood-brain barrier permeability: Preparation, biodistribution studies, and improved brain uptake via neuropeptide conjugation. J Am Chem Soc. 2014; 136:449–457. [PubMed: 24320878]
53. Pérez-Campaña C, et al. Production of 18 F-Labeled Titanium Dioxide Nanoparticles by Proton Irradiation for Biodistribution and Biological Fate Studies in Rats. Part Part Syst Charact. 2013; 31:134–142.
54. Zhu J, et al. Rapid 18F-labeling and loading of PEGylated gold nanoparticles for in vivo applications. Bioconjug Chem. 2014; 25:1143–1150. [PubMed: 24807200]
55. Di Mauro PP, Gómez-Vallejo V, Baz Maldonado Z, Llop Roig J, Borrós S. Novel 18 F Labeling Strategy for Polyester-Based NPs for in Vivo PET-CT Imaging. Bioconjug Chem. 2015; 150309143002009. doi: 10.1021/acs.bioconjchem.5b00040
56. Liu TW, MacDonald TD, Shi J, Wilson BC, Zheng G. Intrinsically copper-64-labeled organic nanoparticles as radiotracers. Angew Chemie - Int Ed. 2012; 51:13128–13131.
57. Gao F, et al. Ultrasmall [64 Cu] Cu Nanoclusters for Using Accurate Positron Emission. ACS Appl Mater Interfaces. 2015; 9:4976–4986.
58. Zhang XD, et al. Ultrasmall Au10–12(SG)10–12 nanomolecules for high tumor specificity and cancer radiotherapy. Adv Mater. 2014; 26:4565–4568. [PubMed: 24817169]
59. Luehmann HP, et al. PET/CT Imaging of Chemokine Receptors in Inflammatory Atherosclerosis Using Targeted Nanoparticles. J Nucl Med. 2016; doi: 10.2967/jnumed.115.166751
60. Chen F, et al. In Vivo Integrity and Biological Fate Mesoporous Silica Nanoparticles. 2015
61. Kaittanis C, et al. Multifunctional MRI/PET Nanobeacons Derived from the In situ Self-Assembly of Translational Polymers and Clinical Cargo through Coalescent Intermolecular Forces. Nano Lett. 2015; acs.nanolett.5b03370. doi: 10.1021/acs.nanolett.5b03370
62. Perez-Medina C, et al. PET Imaging of Tumor-Associated Macrophages with 89Zr-labeled HDL Nanoparticles. J Nucl Med. 2015; 56:1272–1278. [PubMed: 26112022]
63. Normandin MD, et al. Heat-Induced Radiolabeling of Nanoparticles for Monocyte Tracking by PET. Angew Chemie. 2015; 127:13194–13198.
64. Li K, et al. Anti-MET ImmunoPET for Non-Small Cell Lung Cancer Using Novel Fully Human Antibody Fragments. Mol Cancer Ther. 2014; 13:2607–17. [PubMed: 25143449]
65. Phillips E, et al. Clinical translation of an ultrasmall inorganic optical-PET imaging nanoparticle probe. 2014; 6:1–10.
66. Zanzonico P. Principles of Nuclear Medicine Imaging: Planar, SPECT, PET, Multi-modality, and Autoradiography Systems. Radiat Res. 2012; 177:349–364. [PubMed: 22364319]
67. Liberatore M, et al. Effect of External Magnetic Field on IV 99m Tc-Labeled Aminosilane-Coated Iron Oxide Nanoparticles: Demonstration in a Rat Model Special Report. 2015; 40
68. Xue S, et al. 99mTc-Labeled Iron Oxide Nanoparticles for Dual-Contrast (T1/T2) Magnetic Resonance and Dual-Modality Imaging of Tumor Angiogenesis. J Biomed Nanotechnol. 2015; 11:1027–1037. [PubMed: 26353592]

69. Shanehsazzadeh S, et al. Monoclonal antibody conjugated magnetic nanoparticles could target MUC-1-positive cells in vitro but not in vivo. Contrast Media Mol Imaging. 10:225–36. [PubMed: 25327822]
70. Locatelli E, et al. Targeted delivery of silver nanoparticles and alisertib: in vitro and in vivo synergistic effect against glioblastoma. Nanomedicine. 2014; 9:839–849. [PubMed: 24433240]
71. Morales-Avila E, et al. Multimeric System of Tc-99m-Labeled Gold Nanoparticles Conjugated to c{[}RGDfK(C)] for Molecular Imaging of Tumor alpha(v)beta(3) Expression. Bioconjug Chem. 2011; 22:913–922. [PubMed: 21513349]
72. Tsuchimochi M, Hayama K, Toyama M, Sasagawa I, Tsubokawa N. Dual-modality imaging with 99mTc and fluorescent indocyanine green using surface-modified silica nanoparticles for biopsy of the sentinel lymph node: an animal study. EJNMMI Res. 2013; 3:33. [PubMed: 23618132]
73. Seo Y, et al. Mapping of Lymphatic Drainage from the Prostate Using Filtered 99mTc-Sulfur Nanocolloid and SPECT/CT. J Nucl Med. 2011; 52:1068–1072. [PubMed: 21680690]
74. Bradbury MS, Pauliah M, Zanzonico P, Wiesner U, Patel S. Intraoperative mapping of sentinel lymph node metastases using a clinically translated ultrasmall silica nanoparticle. Wiley Interdiscip Rev Nanomedicine Nanobiotechnology n/a–n/a. 2015; doi: 10.1002/wnan.1380
75. Zhu H, et al. Design, synthesis and evaluation of dual-modality glyco-nanoparticles for tumor imaging. Molecules. 2013; 18:6425–6438. [PubMed: 23722731]
76. Zhang R, et al. Annexin A5-conjugated polymeric micelles for dual SPECT and optical detection of apoptosis. J Nucl Med. 2011; 52:958–964. [PubMed: 21571801]
77. Mulvey JJ, et al. Synthesis, pharmacokinetics, and biological use of lysine-modified single-walled carbon nanotubes. 2014:4245–4255.
78. Hoffman D, et al. Intrinsically radiolabelled [59 Fe] -SPIONs for dual MRI/radionuclide detection. 2014; 4:548–560.
79. Robertson R, et al. Optical imaging of Cerenkov light generation from positron-emitting radiotracers. Phys Med Biol. 2009; 54:N355–N365. [PubMed: 19636082]
80. Dothager RS, Goiffon RJ, Jackson E, Harpstrite S, Piwnica-Worms D. Cerenkov radiation energy transfer (CRET) imaging: A novel method for optical imaging of PET isotopes in biological systems. PLoS One. 2010; 5:e13300. [PubMed: 20949021]
81. Liu H, et al. Radiation-luminescence-excited quantum dots for in vivo multiplexed optical imaging. Small. 2010; 6:1087–1091. [PubMed: 20473988]
82. Hu H, et al. PET and NIR optical imaging using self-illuminating (64)Cu-doped chelator-free gold nanoclusters. Biomaterials. 2014; 35:9868–76. [PubMed: 25224367]
83. Sun X, et al. Self-Illuminating 64Cu-Doped CdSe/ZnS Nanocrystals for in Vivo Tumor Imaging. J Am Chem Soc. 2014; 136:1706–1709. [PubMed: 24401138]
84. Black KCL, et al. Radioactive 198Au-doped nanostructures with different shapes for in vivo analyses of their biodistribution, tumor uptake, and intratumoral distribution. ACS Nano. 2014; 8:4385–4394. [PubMed: 24766522]
85. Thorek DLJ, Ogirala A, Beattie BJ, Grimm J. Quantitative imaging of disease signatures through radioactive decay signal conversion. Nat Med. 2013; 19:1345–50. [PubMed: 24013701]
86. Sharma H, Mishra PK, Talegaonkar S, Vaidya B. Metal nanoparticles: a theranostic nanotool against cancer. Drug Discov Today. 2015; 00:1–9.
87. Hong H, et al. Red fluorescent zinc oxide nanoparticle: A novel platform for cancer targeting. ACS Appl Mater Interfaces. 2015; 7:3373–3381. [PubMed: 25607242]
88. Sun M, et al. Highly stable intrinsically radiolabeled indium-111 quantum dots with multidentate zwitterionic surface coating: dual modality tool for biological imaging. J Mater Chem B. 2014; 2:4456.
89. Ai F, Ferreira CA, Chen F, Cai W. Engineering of radiolabeled iron oxide nanoparticles for dual-modality imaging. Wiley Interdiscip Rev Nanomedicine Nanobiotechnology n/a–n/a. 2015; doi: 10.1002/wnan.1386
90. Chakravarty R, et al. Intrinsically germanium-69-labeled iron oxide nanoparticles: Synthesis and in-vivo dual-modality PET/MR zimaging. Adv Mater. 2014; 26:5119–5123. [PubMed: 24944166]

91. Felber M, Alberto R. ^{99m}Tc radiolabelling of Fe_3O_4–Au core–shell and Au–Fe_3O_4 dumbbell-like nanoparticles. Nanoscale. 2015; 7:6653–6660. [PubMed: 25797603]
92. Paik T, et al. Shape-Controlled Synthesis of Isotopic Yttrium-90 Labeled Rare Earth Fluoride Nanocrystals for Multimodal Imaging. ACS Nano. 2015; 150808110701005. doi: 10.1021/acsnano.5b03355
93. Rieffel J, et al. Hexamodal Imaging with Porphyrin-Phospholipid-Coated Upconversion Nanoparticles. 2015; :1785–1790. DOI: 10.1002/adma.201404739
94. Quick AM, Lo SS, Mayr Na, Kim EY. Radiation therapy for intrahepatic malignancies. Expert Rev Anticancer Ther. 2009; 9:1511–21. [PubMed: 19828012]
95. Lee DS, Im H-J, Lee Y-S. Radionanomedicine: widened perspectives of molecular theragnosis. Nanomedicine Nanotechnology, Biol Med. 2015; 11:795–810.
96. McLaughlin MF, et al. Gold Coated Lanthanide Phosphate Nanoparticles for Targeted Alpha Generator Radiotherapy. PLoS One. 2013; 8:2–9.
97. Vilchis-Juárez A, et al. Molecular targeting radiotherapy with Cyclo-RGDfK(C) peptides conjugated to 177Lu-labeled gold nanoparticles in tumor-bearing mice. J Biomed Nanotechnol. 2014; 10:393–404. [PubMed: 24730235]
98. Satterlee AB, Yuan H, Huang L. A radio-theranostic nanoparticle with high specific drug loading for cancer therapy and imaging. J Control Release. 2015; 217:170–182. [PubMed: 26341695]
99. Bogdanov AA, et al. Gold Nanoparticles Stabilized with MPEG-Grafted Poly(L-lysine): in Vitro and in Vivo Evaluation of a Potential Theranostic Agent. Biocordinate Chem. 2015; 26:39–50.
100. Das M, Datir SR, Singh RP, Jain S. Augmented anticancer activity of a targeted, intracellularly activatable, theranostic nanomedicine based on fluorescent and radiolabeled, methotrexate-folic acid-multiwalled carbon nanotube conjugate. Mol Pharm. 2013; 10:2543–2557. [PubMed: 23683251]

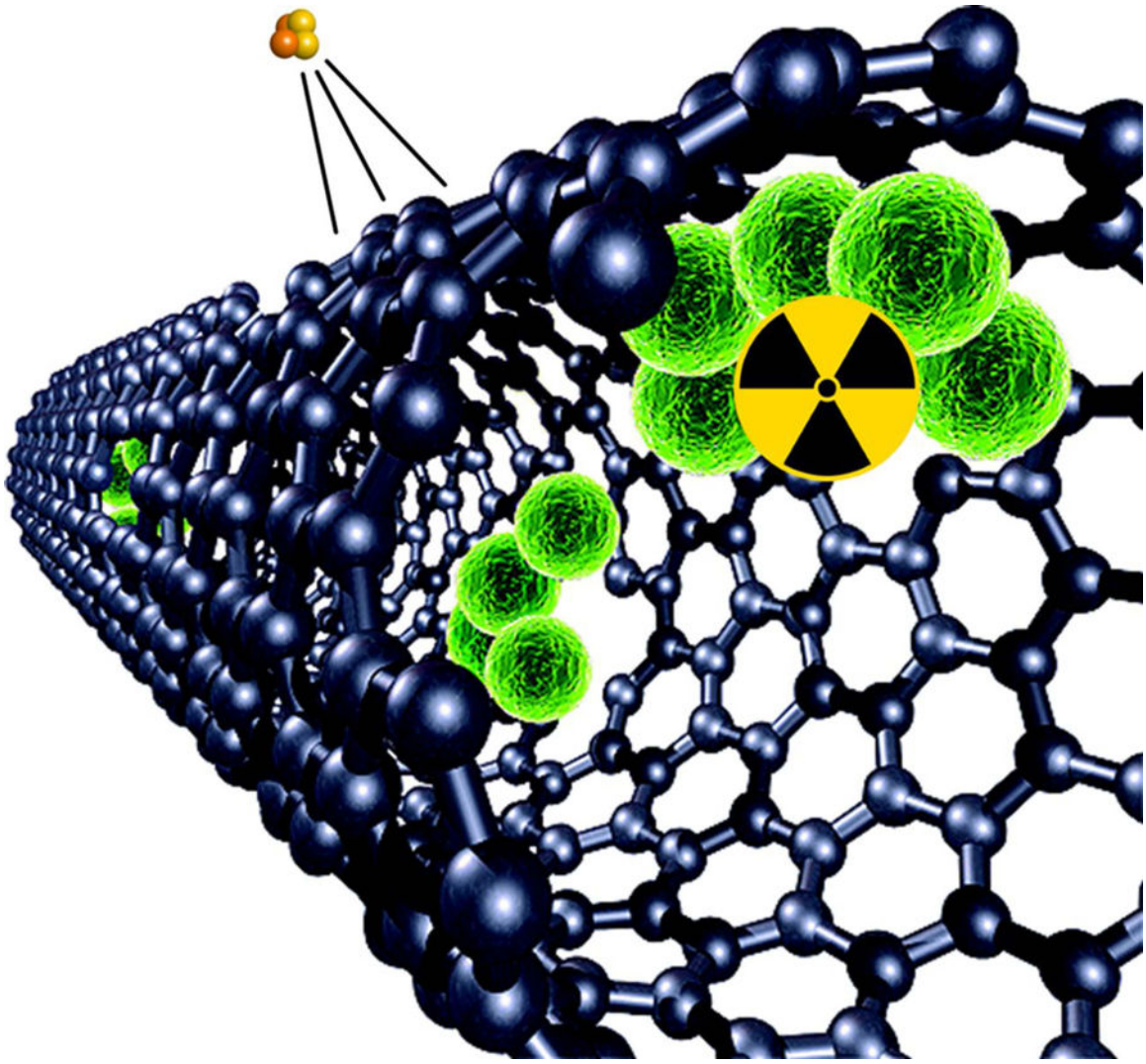

Figure 1.

Three modes of radiation decay: α, β, and γ. Alpha decay is characterized by the ejection of a He^{2+} atom during decay. Beta decay occurs by the ejection of an electron or positron. The beta decay depicted here is for the positron with simultaneous neutrino ejection. In gamma decay, a high energy photon is generated as the atom relaxes to a lower energy state.

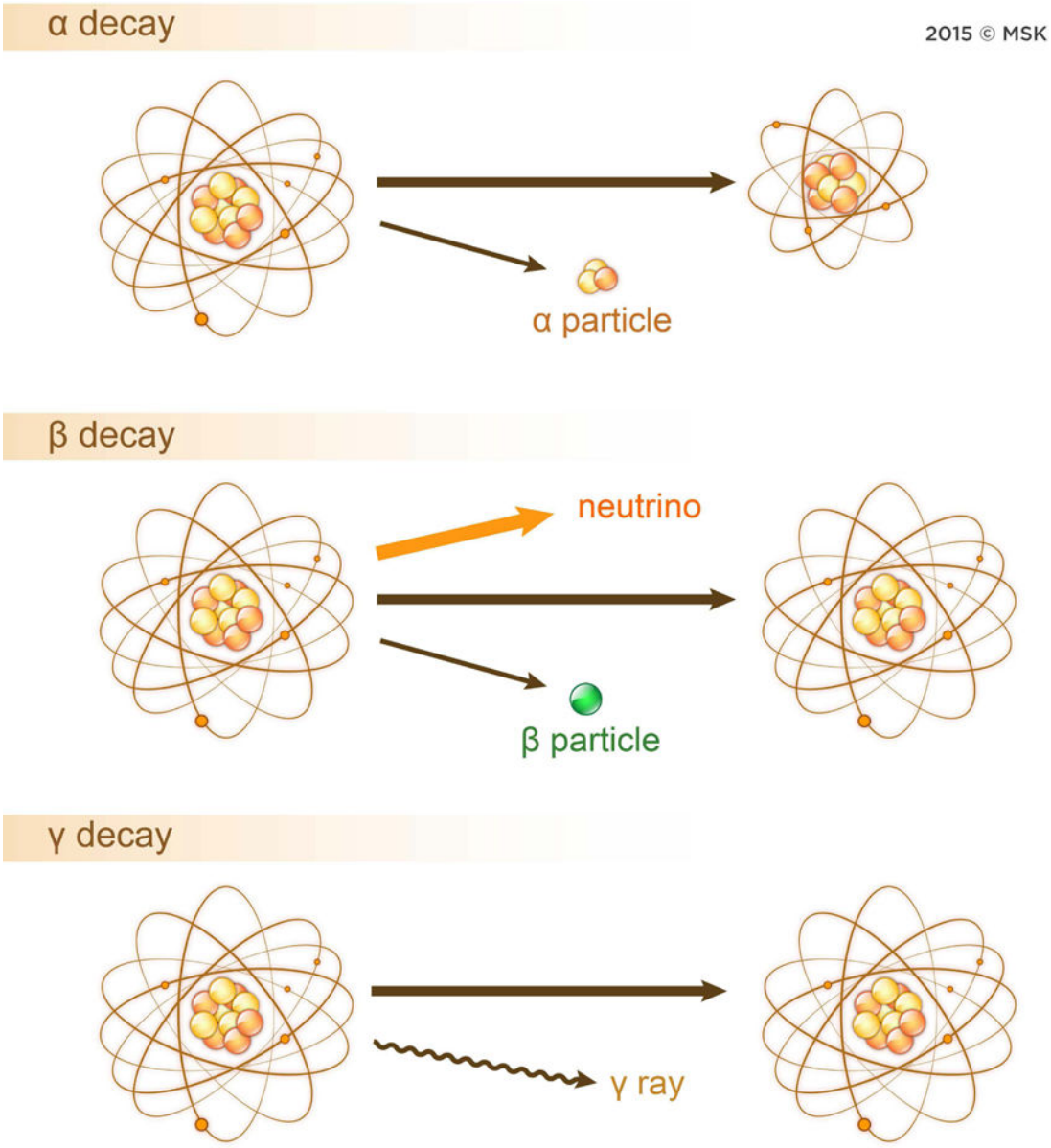

Figure 2.

Four methods of radiolabeling nanoparticles. A) Traditional chelators are chemically conjugated to the surface to serve as sites for radiometal attachment. B) Chelator free radiolabeling method whereby radiometal is directly attached to the nanoparticle surface. C) Direct bombardment of a suitable nanoparticle atom by neutron or proton to yield a radiolabeled nanoparticle. No chelator nor surface chemistry required for radiolabeling. D) Direct synthesis methods whereby cold and hot precursors can be added to produce a nanoparticle with radioisotopes embedded into the nanoparticle lattice.

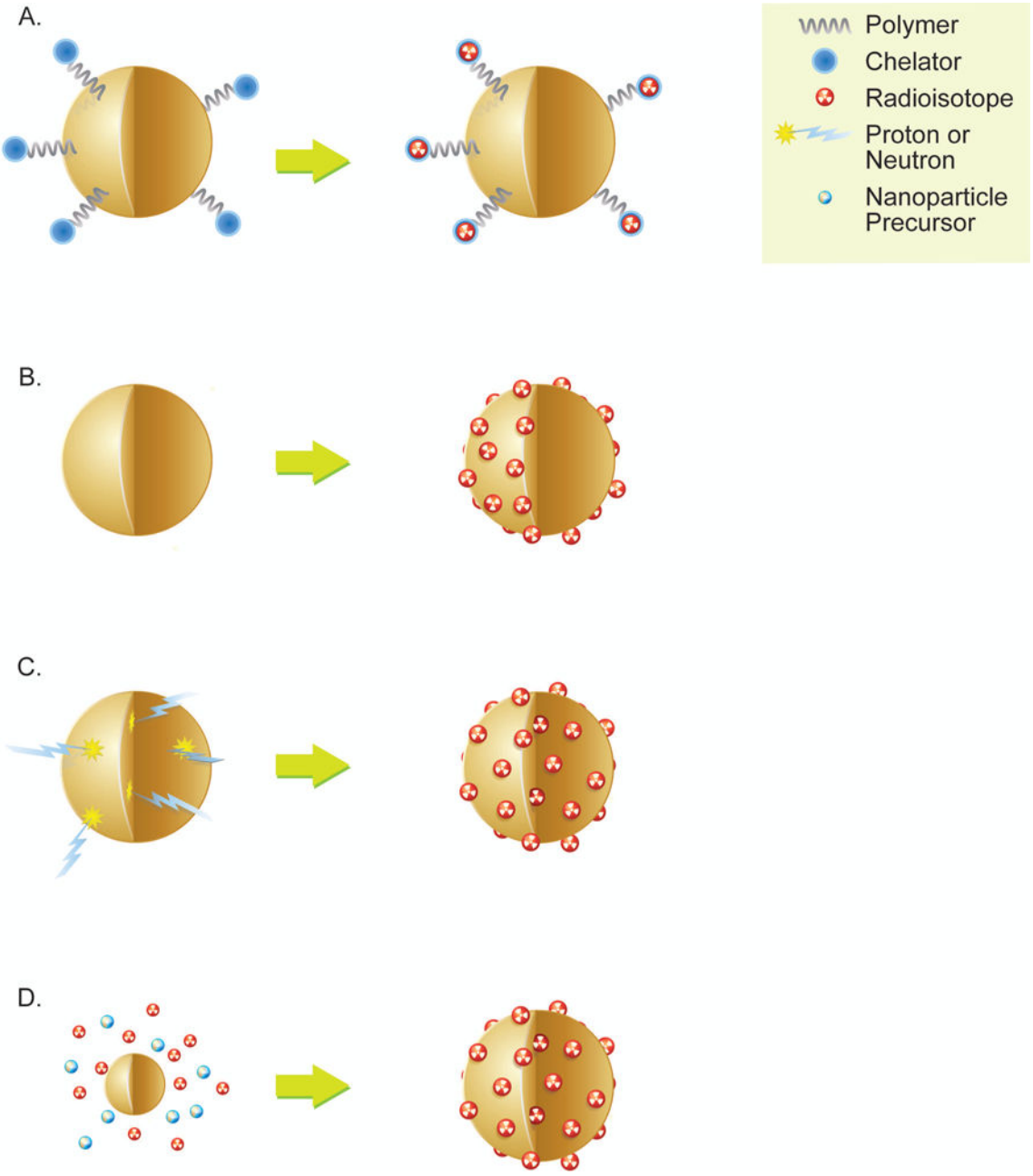

Figure 3.

Representation of ^{225}Ac@GNT construct. Green represents Gd^{3+} ions, yellow with radioactive symbol represents $^{225}Ac^{3+}$ ion, and orange and yellow cluster represents emitted α particle. Reprinted with permission from The Journal of Nuclear Medicine (2015;56:897–900)

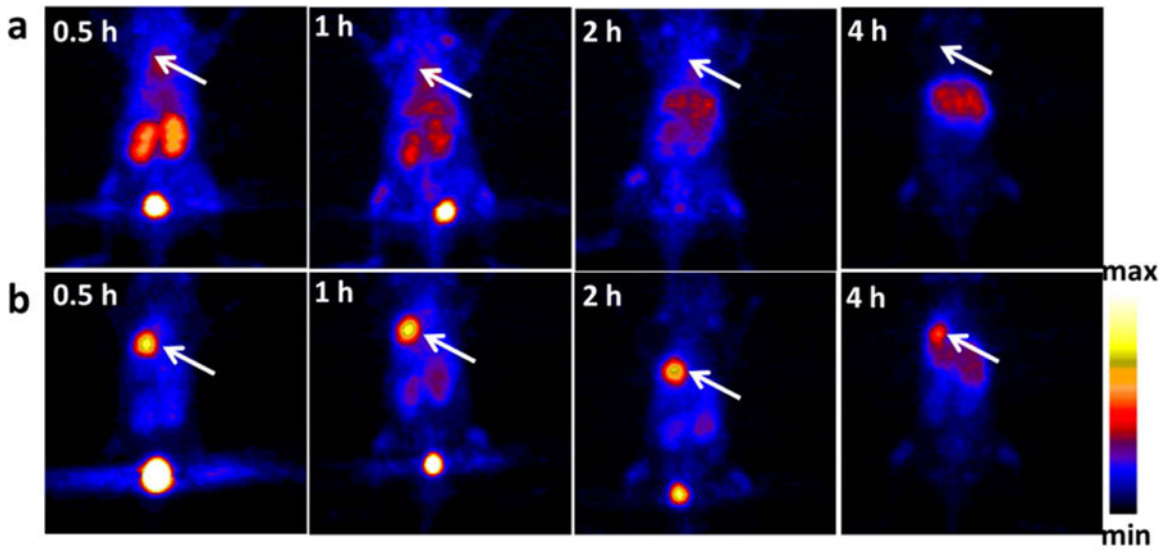

Figure 4.

In vivo PET imaging and biodistribution. Representative PET images of coronal single slices on orthotopic A549 lung tumor bearing mice after intravenous injection of 6.7 MBq of [^{64}Cu]CuNC@BSA (a) and [^{64}Cu]CuNC@BSA-LHRH (b). Images were acquired at 0.5, 1, 2, and 4 h. White arrows indicate the lung tumor. Reprinted and adapted with permission from Gao, F. *et al.* Ultrasmall [^{64}Cu] Cu Nanoclusters for Using Accurate Positron Emission. *ACS Appl. Mater. Interfaces* **9**, 4976–4986 (2015). Copyright 2015 American Chemical Society.

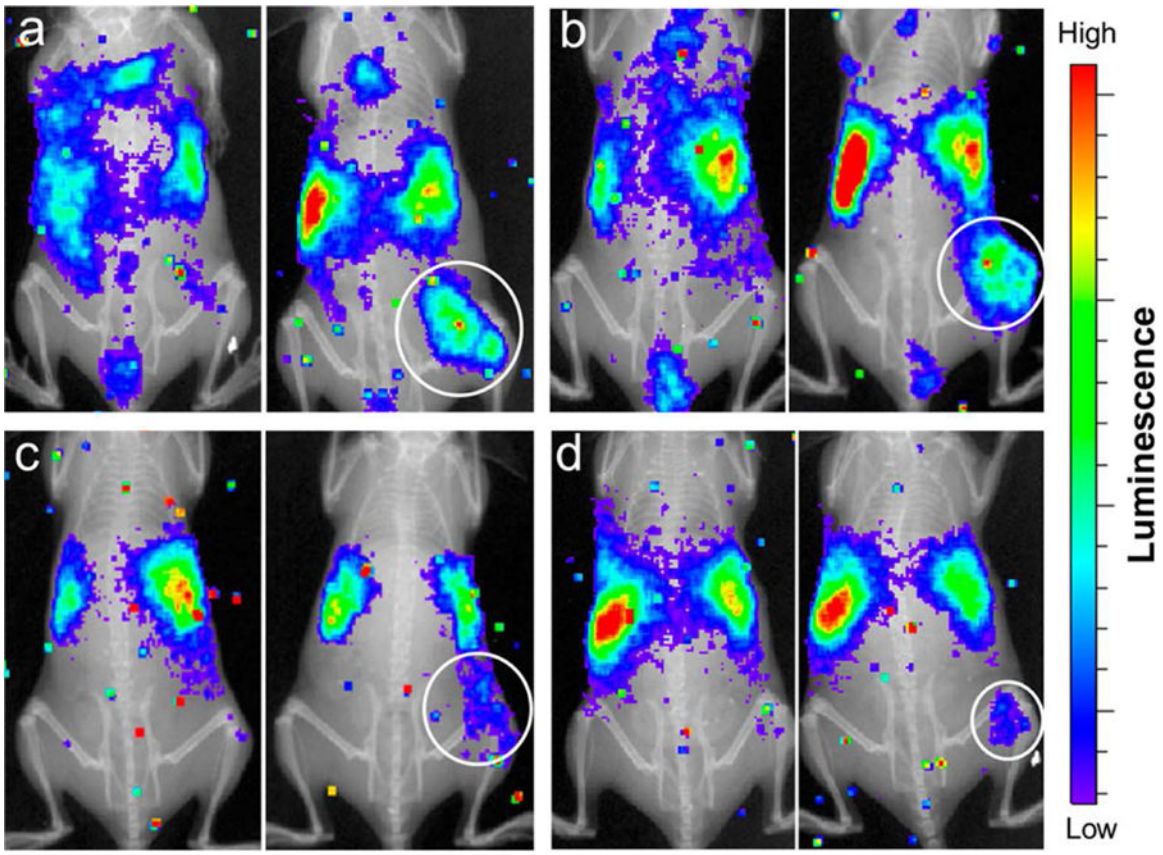

Figure 5.

Co-registered in vivo luminescence and X-ray images of the tumor-bearing mice at 1 h (left panel) and 24 h (right panel) post injection of the different types of 198Au-incorporated nanostructures: (a) nanospheres, (b) nanodisks, (c) nanorods, and (d) cubic nanocages. Reprinted with permission from Black, Kvar C. L. *et al.; ACS Nano* **2014**, 8, 4385–4394. Copyright © 2014 American Chemical Society

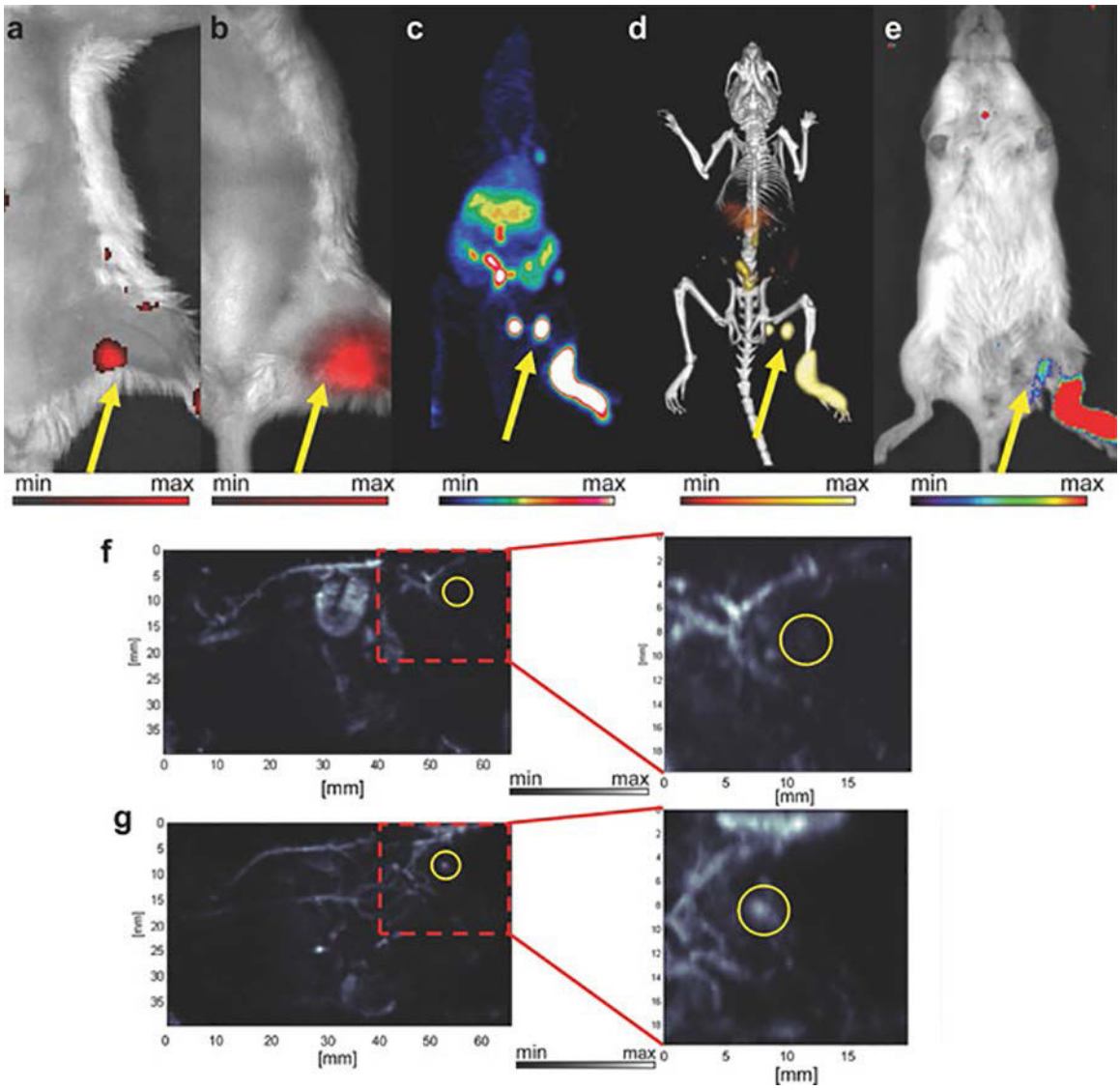

Figure 6.

In vivo lymphatic imaging using PoP-UCNPs in mice. PoP-UCNPs were injected in the rear left footpad and imaged in six modalities 1 h post-injection. Accumulation of PoP-UCNPs in the first draining lymph node is indicated with yellow arrows. a) Traditional FL and b) UC images with the injection site cropped out of frame. c) Full anatomy PET, d) merged PET/CT, and e) CL images. f) PA images before and g) after injection show endogenous PA blood signal compared to the contrast enhancement that allowed visualization of the previously undetected lymph node. Reprinted with permission from Rieffel, J. *et al.* (2015), Hexamodal Imaging with Porphyrin-Phospholipid-Coated Upconversion Nanoparticles. Adv. Mater., 27: 1785–1790.

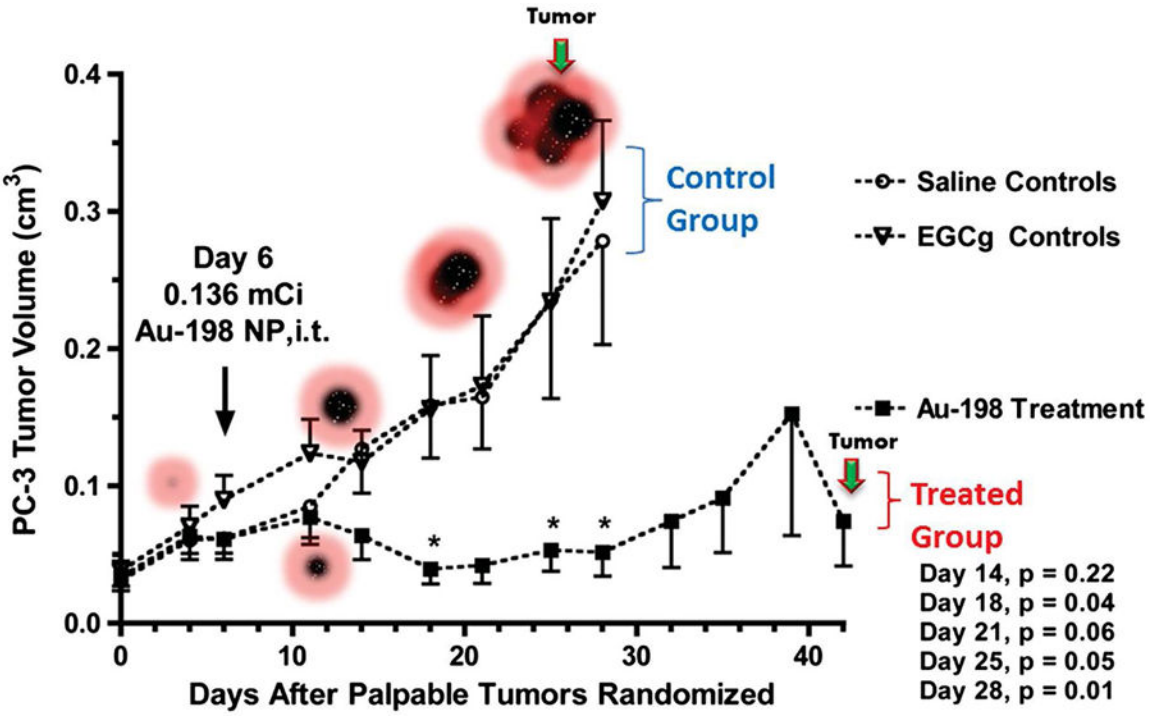

Figure 7.

Tumor therapy using GA-198AuNPs. (A) Therapeutic efficacy of GA-198AuNPs in prostate tumor–bearing SCID mice. Subcutaneous tumors were generated in SCID mice by PC-3 engraftment. Mice bearing palpable tumors were randomized for treatment (n = 7) and control (n = 7) groups followed by intratumoral (IT) injections of GA-198AuNPs (408 μCi per animal) or DPBS, respectively. Graph represents mean tumor volume following 30 days of treatment. (B) TEM image showing uptake of GA- AuNPs in PC-3 prostate cancer cells. Reprinted with permission from Shukla, R. et al. Laminin receptor specific therapeutic gold nanoparticles (198AuNP-EGCg) show efficacy in treating prostate cancer. Proc. Natl. Acad. Sci. 109, 12426–12431 (2012).